energies

MDPI

Article

Laboratory Study of Liquid Nitrogen Cryo-Fracturing as an Environmentally Friendly Approach for Coalbed Methane (CBM) Reservoirs

Sotirios Nik. Longinos [1,*], Alina Serik [2], Emil Bayramov [1,*], Medet Junussov [1], Dastan Begaliyev [1] and Randy Hazlett [1]

[1] School of Mining and Geosciences, Nazarbayev University, Astana 010000, Kazakhstan; medet.junussov@nu.edu.kz (M.J.); dastan.begaliyev@nu.edu.kz (D.B.); randy.hazlett@nu.edu.kz (R.H.)
[2] School of Engineering and Digital Sciences, Nazarbayev University, Astana 010000, Kazakhstan; alina.serik@nu.edu.kz
* Correspondence: sotirios.longinos@nu.edu.kz (S.N.L.); emil.bayramov@nu.edu.kz (E.B.)

Abstract: This study evaluated two distinct cryo-fracturing techniques using liquid nitrogen (LN_2). The evaluation included tests for peak compression strength, acoustic emission, and energy absorption. The experiments compared single-exposure freezing time (FT) and multiple-exposure freezing–thawing cycle (FTC) processes on dried specimens. The outcomes indicated that FTC experiments demonstrated lower uniaxial compression stress (UCS) values compared to FT experiments because, during the thawing phase, the ice inside the pores reverts to liquid as the temperature rises. The difference between average baseline experiments versus FT180 and FTC6 indicated a reduction in stress of 14.5% and 38.5%, respectively. The standard error of our experiments ranged from 0.58% for FT60 to 5.35% for FTC6. The damage factor follows a downward trend in both FT and FTC experiments as the time of LN_2 treatment augments. The amount of energy that can be absorbed in elastic or plastic deformation before failure is less for FTC specimens with the same total LN_2 exposure time. Samples undergoing the freezing time process demonstrate a greater and denser quantity of acoustic emissions in comparison to freezing–thawing cycle processes, suggesting a positive correlation with uniaxial compressive strength outcomes. The large network of fractures formed by the FTC and PFTC techniques indicated that they have the greatest potential as stimulation approaches. The engineering results were improved by adding the geological context, which is essential to apply these findings to coals that have comparable origins.

Keywords: LN_2 fracturing; unconfined test; coalbed methane; immersion tests

check for updates

Citation: Longinos, S.N.; Serik, A.; Bayramov, E.; Junussov, M.; Begaliyev, D.; Hazlett, R. Laboratory Study of Liquid Nitrogen Cryo-Fracturing as an Environmentally Friendly Approach for Coalbed Methane (CBM) Reservoirs. *Energies* **2024**, *17*, 2359. https://doi.org/10.3390/en17102359

Academic Editors: Shu Tao and Dameng Liu

Received: 14 March 2024
Revised: 16 April 2024
Accepted: 30 April 2024
Published: 14 May 2024

Copyright: © 2024 by the authors. Licensee MDPI, Basel, Switzerland. This article is an open access article distributed under the terms and conditions of the Creative Commons Attribution (CC BY) license (https://creativecommons.org/licenses/by/4.0/).

1. Introduction

With the growth of public energy demand, the consumption of coal, oil, and gas to produce energy has shown to be significant in BRICS countries [1]. For example, the BRICS Energy Report suggests that the total coal consumption for these countries hit a level of 5217 metric tons in 2019, which is three times higher than the level of consumption in 1990 [2]. Oil consumption has shown a similar trend, with a growth of approximately 77.5% in three decades. In addition, 910 billion cubic meters of gas were consumed in 2019, in contrast to 506 billion cubic meters in 1990. All these statistics show a strong dependency on fossil fuel-driven energy sources [1]. As per the BRICS Energy Report, fossil fuels will remain a major energy source until the end of 2040 [2]. Overall, the worldwide trend also shows a dependence on energy driven by fossil fuels, which accounts for up to 80% [3–5]. Despite its low cost of production and availability, fossil fuels negatively impact the environment [6–8]. Therefore, developing new technologies in the oil and gas industry is crucial to producing more fossil fuels with a minimum effect on the environment. In recent years, unconventional natural gas production potential has been unlocked through

hydraulic fracturing to increase reservoir contact for shale gas or coal seam gas extraction [9]. Hydraulic stimulation uses water pressure to exceed rock strength and the addition of chemicals to reduce friction and control the extent of fractures [10]. Added chemicals give rise to environmental concerns over ground contamination and wastewater disposal [11–13]. Thus, reservoir stimulation with less environmental risks is of merit.

Due to the efficacy of fracturing applications, unconventional methods of extracting gas from formations prosper in the oil and gas industry [14]. One of the solutions for the water pollution problem might be hydraulic fracturing using LN_2 [15,16]. The high temperature of geological formations and low temperature of injected liquid nitrogen leads to the formation of thermal stress cracks to improve the migration potential of gas [17]. In contrast to conventional hydraulic fracturing, which uses a lot of water and chemicals, there are currently waterless fracturing technologies that also include natural gas fracturing [18–20], blasting fracturing [21–23], and low-temperature CO_2 fracturing [24–26], which have their own advantages and drawbacks. In gas fracturing, blasting fracturing, and CO_2 low-temperature fracturing, there is no use of water; hence, there are no chemical exposure risks for contaminated water horizons, and reduced wastewater management is needed [27–32]. On the other hand, there is a connection between increased seismic activity and fracking operations; large-scale infrastructure is needed for fracturing, including pipelines, access to roads, and well pads. Moreover, community disruption through noise traffic and air pollution can create negative impacts on the quality of life [33–38].

The LN_2 hydraulic fracturing has several advantages. First, besides creating new fractures, it also enlarges existing cracks, thereby creating interconnections between fractures, i.e., creating fracture meshes [17,39]. As such, the permeability and porosity of coal formations increase [40,41]. Second, several freezing–thawing cycles may successively subdivide rocks into particles [42,43]. An advantage is that the loose particle debris can act as proppants and prevent the closing of the existing fractures [44–46]. Third, hydraulic fracturing with water can cause clay swellings, leading to formation damage. Cryogenic fracturing does not alter clay and, therefore, is more environmentally friendly [47]. However, despite the advantages of this new technology, several drawbacks and challenges should also be mentioned. First, the low temperature of liquid nitrogen can create structural problems in the wellbore [48]. Second, prolonged injection may be needed due to possible heat transfer problems, affecting fracturing effectiveness. The third technology gap to be mentioned is proppant transport, which limits massive cryogenic stimulation [49,50].

The mechanical characteristics and pore structure of coal rock mass frozen by low-temperature LN_2 have been the subject of much research. After LN_2 freezing–thawing cycles, Li et al. [51–53] subjected water-saturated coal samples to mechanical testing. The alterations seen in mechanical metrics, such as compressive strength, elastic modulus, and Poisson's ratio, suggest that the freezing of LN_2 causes harm to coal's pore structure, hence diminishing its mechanical attributes. Using a scanning electron microscope (SEM) and nuclear magnetic resonance (NMR), Cai et al. [54–56] examined rocks before and after LN_2 freezing. They concluded that the pore structure of rocks undergoes three primary changes following LN_2 freezing: a decrease in pore volume, an extension of micropores, and an increase in pore size. According to Qin et al.'s research [42,57,58], coal is frozen with LN_2 and will have bigger pores and produce new cracks. Additionally, the pace at which pore size increases positively correlates with the duration of LN_2 treatment. In their mechanical experiment, Sandstrom et al. [59] found that the quantity of freezing–thawing cycles on rocks influenced the mechanical characteristics and fissures in the material. It should also be mentioned that the LN_2 process, as the waterless hydraulic fracturing method, has been used by different research groups in shale [41,60,61], carbonate [17,62], sandstone [63,64], and granite [65–67] rocks with successful results as it initiates the mechanical and physical deterioration of the samples of varying mineralogy and composition.

This work explores the changes in pore structure characteristics that are seen in coal samples that are obtained from the Karaganda area after they are exposed to liquid nitrogen (LN_2), which is used as a waterless fracturing method for coalbed methane (CBM) reservoirs. The impact of the length of LN_2 freezing and the frequency of freezing–thawing cycles are examined, considering the timing differences. There is an examination of stress versus time, load versus displacement, absorbed energy, and damage factor versus each process along with acoustic emission (AE) measurements. Moreover, incorporating the geological context enhanced the engineering outcomes, which is a crucial step in translating these findings to coals with similar origins. For the first time, there was a statistical analysis of our outcomes since assessing repeatability and reproducibility is necessary to guarantee the validity of experimental results.

2. Geological Settings in Karaganda Basin

With about 41.3 billion tons of known coal deposits and perhaps up to 4.3 trillion cubic meters of coal bed methane, the Karaganda basin stands out as a major coal-producing basin in central Asia [68–70]. The terrain of the basin is mainly steppes and bare hills. The carbon coal content portion of the basin is about 2000 km^2 and 4000 m deep [71]. A latitudinally oriented asymmetric synclinorium with a depth of around 30 by 120 km is present in the Karaganda coal basin [72,73]. Paleozoic, Mesozoic, and Cenozoic formations make up its geological makeup [74]. Three synclinal troughs are seen in the basin, spaced apart by uplifts that manage many faults that are directed both transversely and longitudinally concerning the direction of the main fold [67,68]. The basin spans 3600 km^2, of which 2000 km^2 is primarily covered by coal occurrences in the Carboniferous formation. The Lower-Middle Jurassic and Lower-Middle Carboniferous strata contain coal deposits [75].

The Karaganda basin's coal seams have a complicated structure and normally have a thickness of 0.7 to 2.5 m, with sporadic reaches of up to 7–8 m. The majority of the coal is hard and humic; around one-third of the coking coals may be concentrated easily, and the remaining coals are classified as power coals because of their high ash level and difficulties in concentration. The ash composition of coal suites differs; the Tentekskaya and Ashliarikskaya suites have a greater ash content (20–45%), while the Dolinskoe (4–15%) and Karaganda (8–25%) suites have lower ash contents. The coals typically have a low sulfur content—rarely more than 1%—and a high phosphorus content—between 0.01% and 0.1%. Gas, fat, fat coking, coking, coking 2, and lean caking coals are among the coals that are ranked according to their degree of metamorphism, considering variables such as volatile matter yield and caking capacity [68]. Brown coals from the Jurassic strata, on the other hand, exhibit volatile matter yields of between 42% and 52% of the combustible mass, ash contents of 15% to 22%, and sulfur contents of 0.01% to 1.2%. These brown coals normally have a working moisture content of 9% to 19% [72,75]. About 10.8 million tons of coal with a gas content of 16–57 cubic meters per ton of coal are produced annually by the mines in the Karaganda coal basin. Approximately 277 million cubic meters of methane are recovered by capture technologies; 242 million cubic meters are retrieved through ventilation, and 35 million cubic meters are extracted through degassing. As of right now, only 12 million cubic meters (or 4.3% of the degassed volume) of methane are being used; the rest is being burned, which adds a great deal to local and worldwide pollution [72].

3. Experimental Procedure

3.1. Synthetic Coal Specimen Preparation

This study employed synthetic coal specimens frequently used as a replacement for coal in experimental tests due to the inability to preserve samples of prescribed geometries as required in many standard geomechanical procedures. It was discovered that these samples had remarkably similar qualities to natural coal and were stable during LN_2 treatments [76–82]. Generally, synthetic coal is made of coal particles, sand, cement, and water. Initially, bulk coal was crushed in three steps using a jaw mill, disk mill, and drum mill to form fine coal powder. After grinding and crushing, the coal particles were sieved.

The water/cement/sand/coal particles ratio was 3:2:1:4 for our specimens. Then, the mixture was poured into cubic molds. After 24 h, the specimens were removed from molds and cured under water for at least a month to ensure strength development. All specimens in the experiments were of equivalent dimensions. Figure 1 shows the procedure of sample preparation with different equipment.

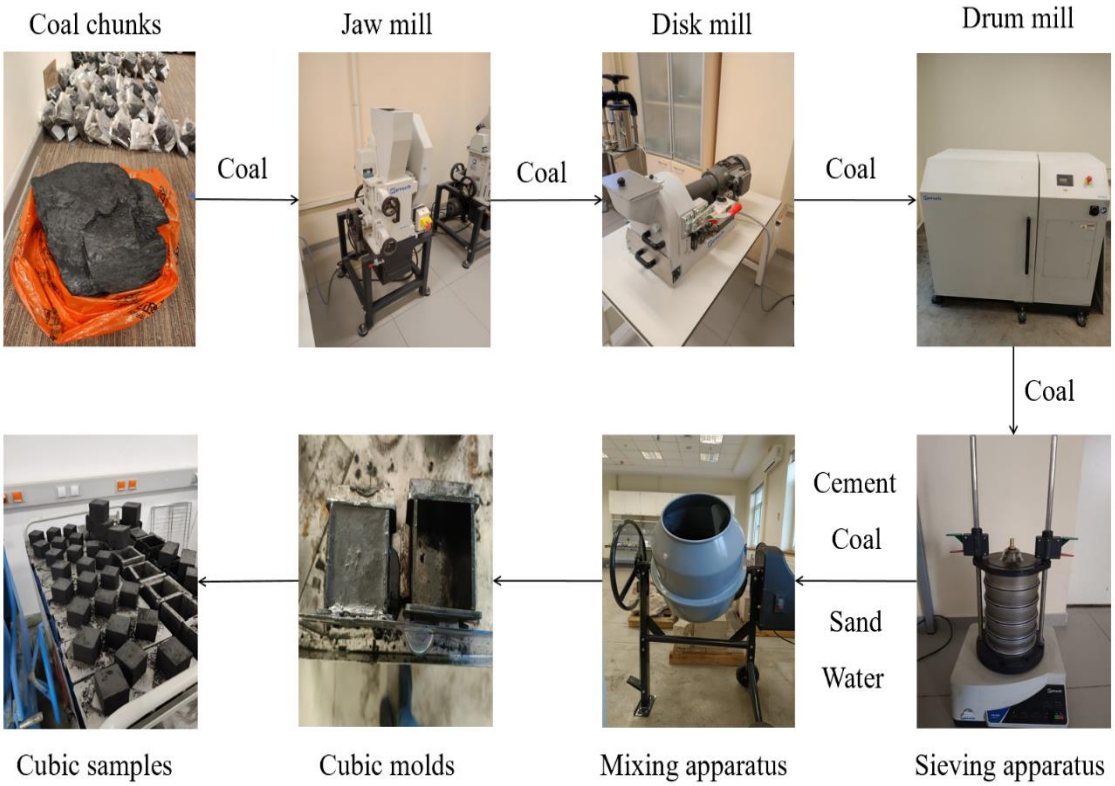

Figure 1. Synthetic coal preparation of cube specimens.

3.2. Test Procedures

The synthetic coal samples for compression tests were 5 × 5 × 5 cm cube blocks. Before the tests, the samples were placed in a drying oven for 48 h at 50 °C temperature to drive out all moisture. Afterward, samples were immersed in LN_2. The LN_2 treatment involved freezing time (FT) and freezing–thawing cycles (FTC). The freezing times tested were 60, 120, and 180 min, and the number of freezing–thawing cycles examined were 2, 4, and 6. In FTC, the samples were frozen for 30 and thawed at room temperature for 30 min at each cycle. Then, the samples were put in a drying oven and preheated for 2 h to the temperature of field conditions, i.e., 50 °C. The experimental process is illustrated in Figure 2. The uniaxial compression test was conducted using a universal testing machine with a servo-hydraulic system, model WAW—1000 D (Jinan XinLuXhang Testing Machine Co., Ltd., Jinan, China), along with an acoustic emission (AE) instrument, model SAEU3H (QingCheng AE Institute (Guangzhou) Co., Ltd. Guangzhou, China).

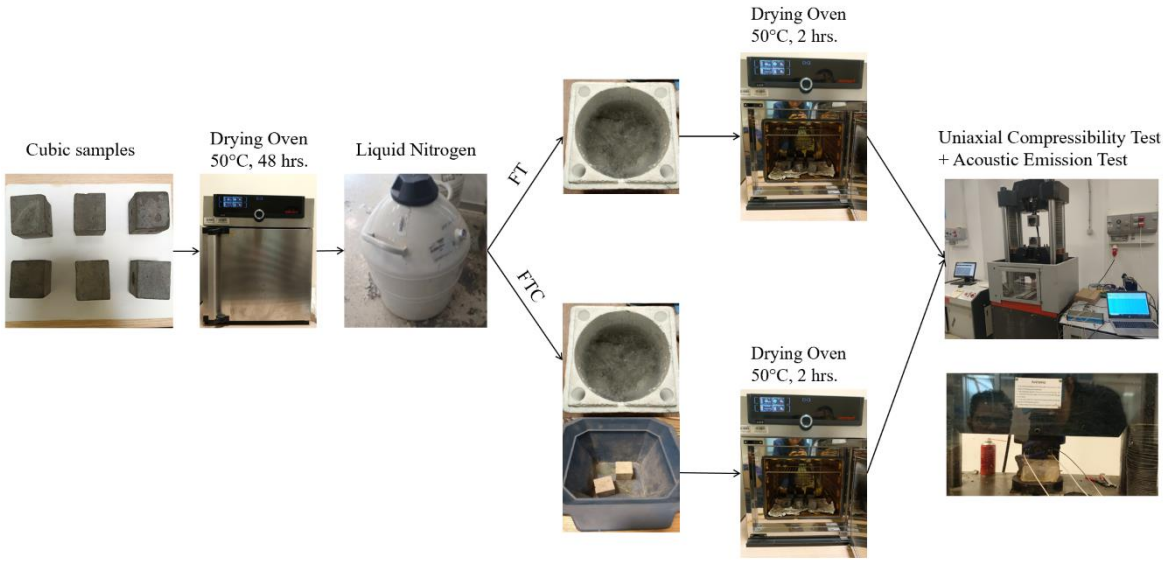

Figure 2. Physical processes in the experimental protocol before examination of our coal specimens.

4. Results and Discussion

4.1. UCT Outcomes

The uniaxial compression test (UCT) was conducted to examine the strength of samples that underwent LN_2 treatment. Figure 3 compares the results of UCT on specimens with freezing time and freezing–thawing cycles of LN_2 treatment. It was found that as the freezing time and number of freezing–thawing cycles increase, the compressive strength of coal blocks decreases significantly, indicating that cryogenic fracturing can stimulate fracture initiation. The highest compressive strength of 3.31 MPa on average was depicted for the control specimen without any treatment, whereas the lowest strength of 2.52 MPa and 1.27 MPa on average was determined for FT180 and FTC6 specimens, respectively. The compressive stress of samples varies for different LN_2 treatment experiments from 3.3% (difference between baseline and FT60 experiment) to 12.9% (difference between baseline and FT180 experiment) for FT experiments and from 7.4% (difference between baseline and FTC2 experiment) to 24% (difference between baseline and FTC6 experiment) for FTC experiments. Additionally, the difference between the successive experimental applications varies from 3.3% (difference between baseline and FT60 experiments) to 14.5% (difference between FT120 and FT180 experiments) for FT experiments, and from 16.6% (difference between baseline and FTC2 experiments) to 38.5% (difference between FTC4 and FTC6 experiments) for FTC specimens. Moreover, Table 1 shows the standard error of UCS peaks, which is between 0.58% and 5.35%, which indicates the accuracy of the research. To better understand the variability and distribution of the data from experiments, statistical tools, namely simple standard deviation, population standard deviation, and the relative standard deviation (RSD) for simple and population standard deviations, were determined. In general, both simple and population standard deviation values are relatively small in the range from 1.16 to 10.69 and 1.01 to 9.26, respectively, indicating consistency among the experimental data. The RSD is another statistical tool that indicates how precise the average of the dataset is. The RSD values for simple and population standard deviation range from 0.36 to 8.40 and 0.31 to 7.27, respectively. The smaller RSD values indicate the accuracy of the observed values. The uniaxial compressive strength with different freezing processes is shown in Figure 4. It can be noticed from Figure 4 that the uniaxial compressive strength of synthetic coal samples mildly decreases linearly with the increase in LN_2 freezing time. However, a significant strength drop is observed in FTC samples, with an increase in the number of cycles.

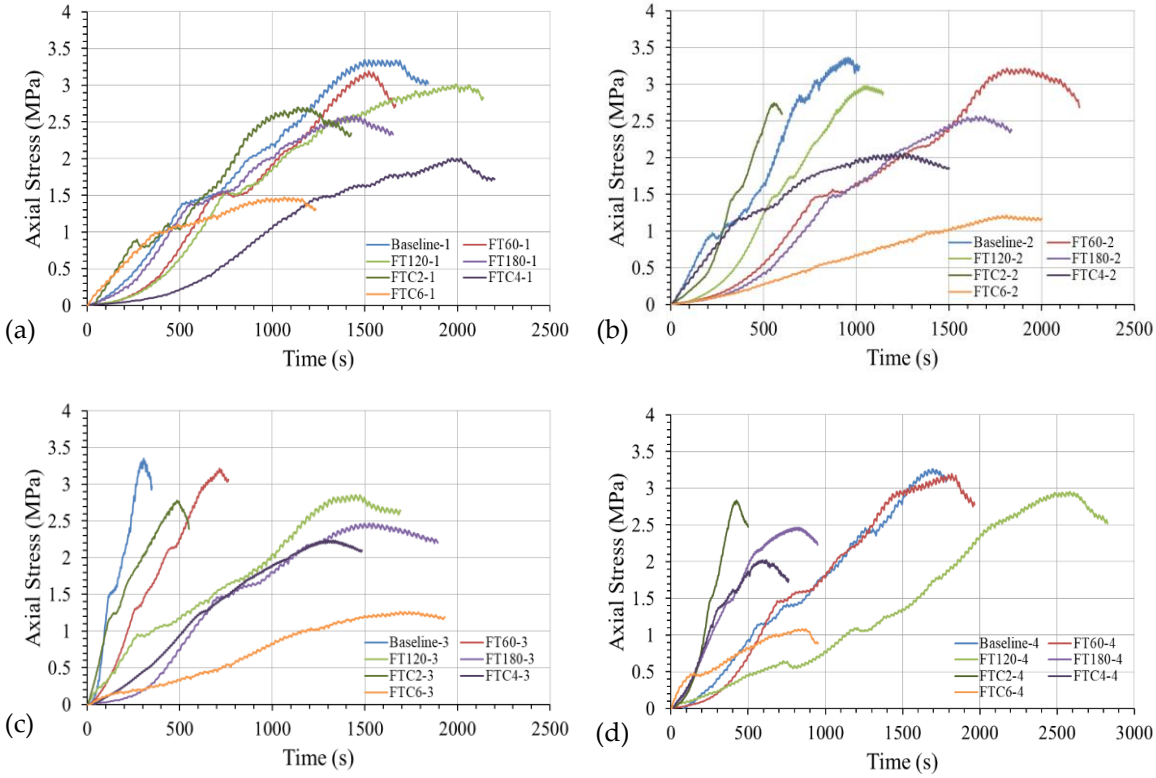

Figure 3. Uniaxial stress vs. time curves. The first try (**a**), second try (**b**), third try (**c**) and fourth try (**d**) of experiments.

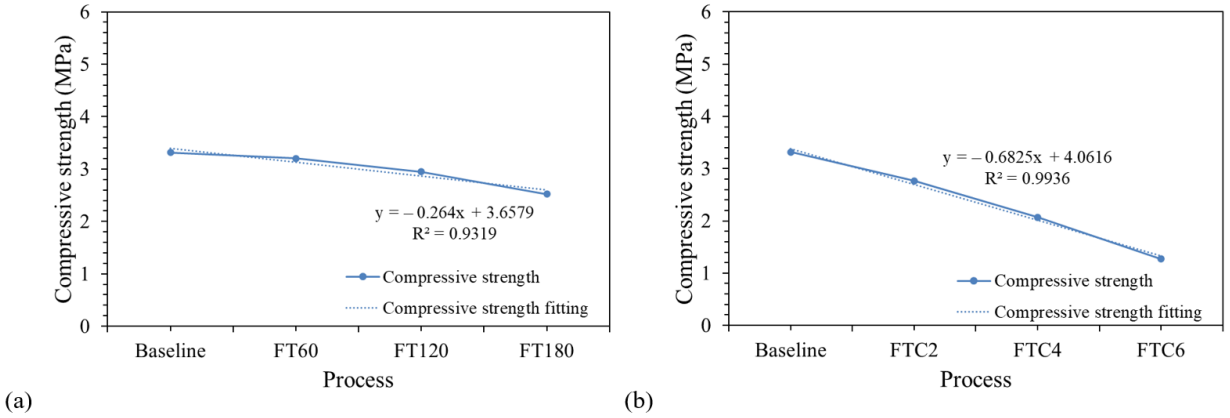

Figure 4. Compression strength vs. FT (**a**) and FTC (**b**) processes.

Table 1. Results from UCT for FT and FTC experiments.

Specimen	Process	UCS Peaks (MPa)	Average (MPa)	Difference between Baseline and Experimental Applications	Difference between Successive Experimental Applications	Standard Error (%)	Simple Standard Deviation (%)	Population Standard Deviation (%)	RSD for Simple Standard Deviation	RSD for Population Standard Deviation
1	Baseline	3.26	3.31	-	-	2.28	4.95	4.29	1.49	1.29
2		3.36								
3		3.35								
4		3.34								
1	FT60	3.19	3.20	3.3	3.3	0.58	1.16	1.01	0.36	0.31
2		3.21								
3		3.21								
4		3.19								

Table 1. *Cont.*

Specimen	Process	UCS Peaks (MPa)	Average (MPa)	Difference between Baseline and Experimental Applications	Difference between Successive Experimental Applications	Standard Error (%)	Simple Standard Deviation (%)	Population Standard Deviation (%)	RSD for Simple Standard Deviation	RSD for Population Standard Deviation
1	FT120	3.01	2.95	7.7	8.0	3.39	6.78	5.87	2.29	1.99
2		2.98								
3		2.85								
4		2.95								
1	FT180	2.46	2.52	12.9	14.5	3.03	6.07	5.26	2.40	2.08
2		2.56								
3		2.46								
4		2.58								
1	FTC2	2.74	2.76	7.4	16.6	2.84	5.68	4.92	2.05	1.77
2		2.71								
3		2.77								
4		2.83								
1	FTC4	2.01	2.06	21.0	25.2	4.09	8.18	7.08	3.95	3.42
2		2.05								
3		2.18								
4		2.02								
1	FTC6	1.21	1.27	24.0	38.5	5.35	10.69	9.26	8.40	7.27
2		1.42								
3		1.26								
4		1.18								

The damage factor can be determined by the following equation:

$$D_F = 1 - \frac{F_c}{F_0}, \quad (1)$$

where D_F is the damage factor, F_c is the maximum fracture load for different LN_2 treatments, and F_0 is the fracture load for the baseline experiment. It can be observed from Figure 5 that the damage factor increased as the freezing time increased for both FT and FTC experiments. In general, the damage factor of FT experiments is less than FTC experiments, indicating a higher extent of fracturing in FTC experiments. For the baseline experiment, the damage factor is equal to 0. In FT experiments, as the freezing time increases, the damage factor gradually rises to the highest value of 0.24 at the 180 min freezing time (FT180). A similar trend is observed for the FTC experiments, where the damage factor increases relatively sharply and notably with a rise to 0.62 at the 6-cycle freezing–thawing experiment (FTC6).

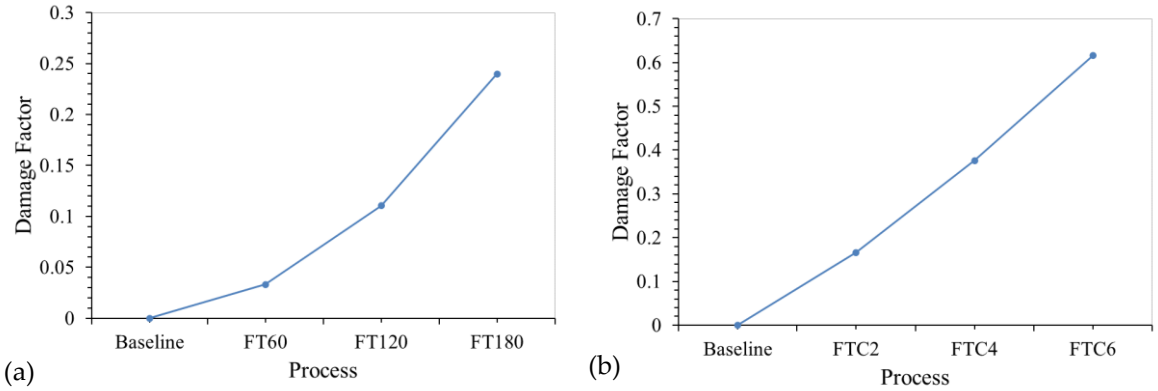

Figure 5. Damage factor vs. process for both FT (**a**) and FTC (**b**) methods.

The decrease in peak uniaxial compressive strength (UCS) is attributed to the freezing and expansion of frost forces within the coal cleats, leading to a reduction in the overall

rock strength at a macroscopic level for both FT and FTC experiments. The processes of mechanical weakening occur at the pore level and are influenced by factors such as grain sorting, pressure, and temperature. It remains unclear whether a specific mechanism prevails over others [50,83,84]. Furthermore, the failure of pore walls and the subsequent clustering of pores contribute to the generation of new fractures and modifications to existing ones. The accumulation of frost heave forces at angular pore terminations results in stress concentration at the tips of fractures, consequently promoting the further extension of these fractures [83]. Finally, the experiments conducted with freezing–thawing processes exhibit lower peak values compared to the freezing time process, consistent with prior research findings [48]. It is suggested that the freezing–thawing cycle process may exert a more significant impact on the growth rate of seep-age pores compared to the freezing time process. Additionally, the repetition of freezing–thawing cycles is observed to play a more substantial role in the creation of large seepage pores [50,85,86]. Furthermore, as the temperature rises during the thawing phase, the ice within the pores transforms back into a liquid phase. This results in the creation of new pathways and newly formed fissures [44,87–89]. The subsequent frost heaving in the subsequent freezing cycle has the potential to damage pore structures that were not previously affected solely by an increase in freezing time [48,90]. Successive freezing–thawing cycles contribute to the formation of associations between cracks, further diminishing the material's strength in macroscopic strength testing [48,50,91].

4.2. Absorbed Energy Outcomes

The Total Absorbed Energy is determined as the work performed by the axial load as shown in the following equation:

$$E_{absorbed} = \int P \times \partial\delta, \tag{2}$$

where P is the axial load and δ is the axial displacement of the coal specimen. The load versus displacement curves illustrated in Figure 6 are used to calculate the absorbed energy. For finite data, the summation symbol replaces the integration symbol, and the trapezoidal rule was used to compute the absorbed energy as shown below:

$$E_{absorbed} = \sum_{i=2}^{n-1} \frac{P_{i+1} + P_{i-1}}{2} \times (\delta_{i+1} - \delta_{i-1}), \tag{3}$$

Figure 7 depicts the absorbed energy of coal samples after various freezing–thawing cycles. It should be emphasized that the absorbed energy was computed as the area up to the peak load because the test time varied for each specimen. As expected, the highest value of the absorbed energy was observed for the baseline specimen with 11.39 J, while the lowest value was detected for the FTC 6 specimen with 2.56 J. Overall, it is clear that the absorbed energy decreases with an increase in freezing time. In addition, almost all specimens of FT and FTC experiments follow the general decreasing trend. For FT experiments, the absorbed energy decreases gradually from 11.39 J to 6.5 J as the freezing time increases to 180 min. As for FTC experiments, the drop in absorbed energy values is noticeable and significant, which is nearly four times less from the baseline to the FTC 6 specimen.

Overall, the graph illustrates the inconsistency between the absorbed energy and compressive strength. In FT experiments, there is a slight reduction between baseline and FT60 experiments, followed by a more intense reduction and finishing with a minor reduction. In FTC experiments, there is a fluctuation similar to FT experiments. In FTC experiments, the behavior is similar to FT but more pronounced. From baseline to FTC2 experiments, there is an obvious reduction, which becomes sharper from FTC2 to FTC4. The reduction remains intense between FTC4 and FTC6, showing different behavior compared to FT experiments. The reason for that behavior is due to liquid that transforms into gas and

expands in the cleats of coal, and the overall macroscopic strength of the rock decreases over a longer time due to the thawing process. An analysis of energy absorption demonstrated a clear decrease in the strength of coal samples as freezing time and freezing–thawing cycles increased. LN_2 treatment caused more cracks and damage to the coal, leading to this decline in strength. Moreover, the absorbed energy values in FTC experiments are lower compared to FT experiments for the same duration of LN_2 treatment across all experiments. Figure 8 shows the sample before and after the compression test.

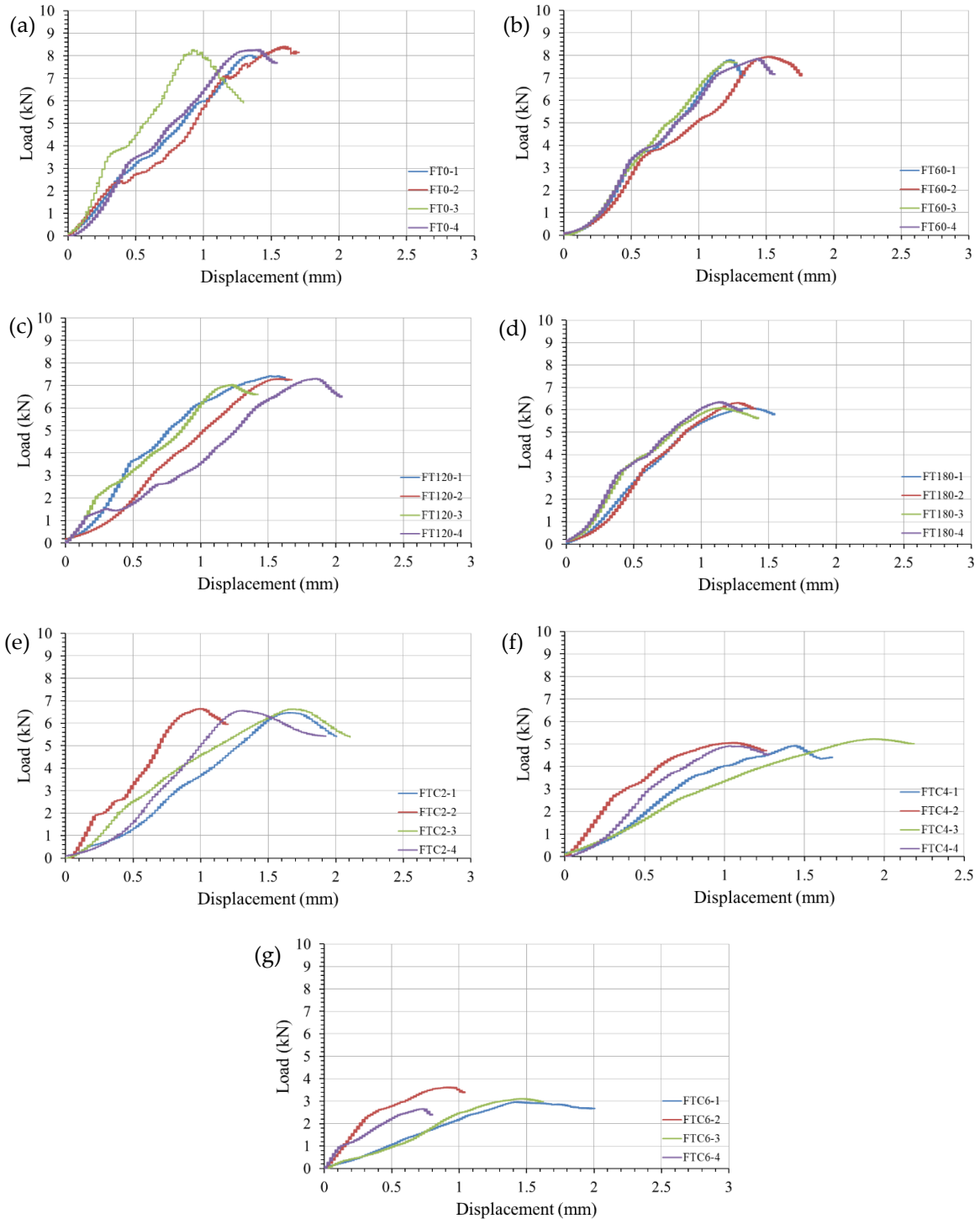

Figure 6. Load vs. displacement curves.

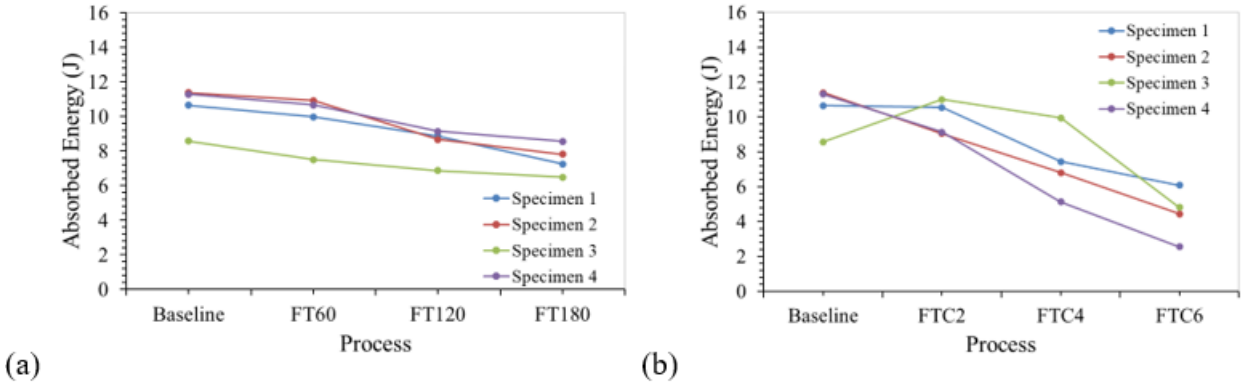

Figure 7. Absorbed energy vs. process curves for FT (**a**) and FTC (**b**) methods.

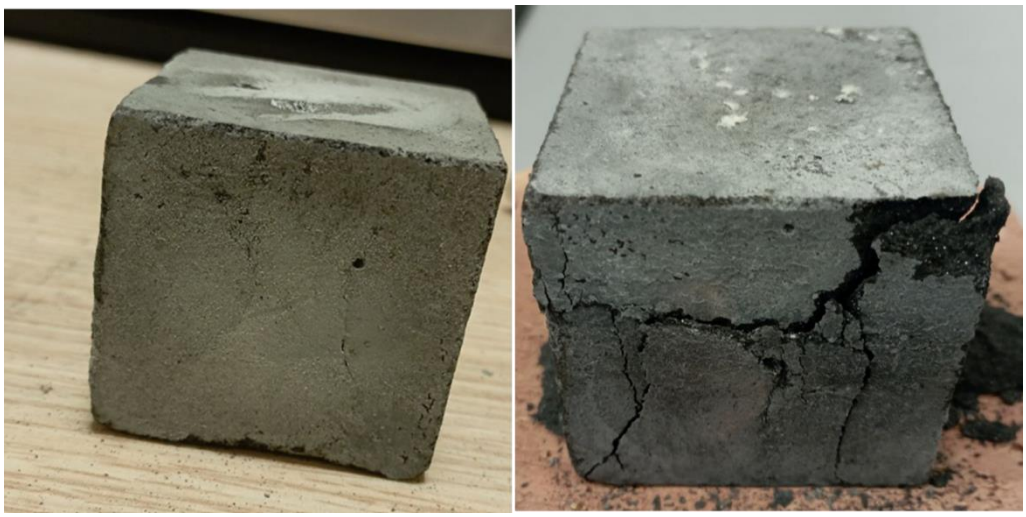

Figure 8. Specimen before compression test (**left**) and specimen after compression test (**right**).

4.3. AE Test Results

During the uniaxial compression test, the applied loads on coal samples cause stress concentration in coal internal fissures, leading to higher strain energy. Therefore, during the loading process, coal samples release elastic waves, known as acoustic emission (AE) signals. The monitoring of AE signals during the uniaxial compression test is crucial in analyzing the damage mechanism of coal under compression. At the initial stage of loading and in the fracture compaction stage, coal samples without LN_2 treatment have relatively lower amplitude frequency. At this stage, fractures and micro-pores in samples start to close and slowly become compacted. With the increase in LN_2 freezing time, frequent and large amplitude AE signals can be observed. At the yield stage, more intense AE signals are generated since cracks start to connect during loading. As the LN_2 fractured coal samples have bigger fractures from treatment, the AE counts suddenly increase, so the cumulative AE counts of the samples become larger. At the failure stage, small fractures develop into large pores, which eventually results in the brittle failure of the coal samples. During the failure, the coal samples experience a release of some stress, which corresponds to the frequent and rapid increase in AE counts in both FT and FTC experiments. Moreover, FT processes exhibit a higher and more dense number of signals compared to the FTC process, indicating a positive correlation with UCT results. Figures 9 and 10 show the results from AE tests.

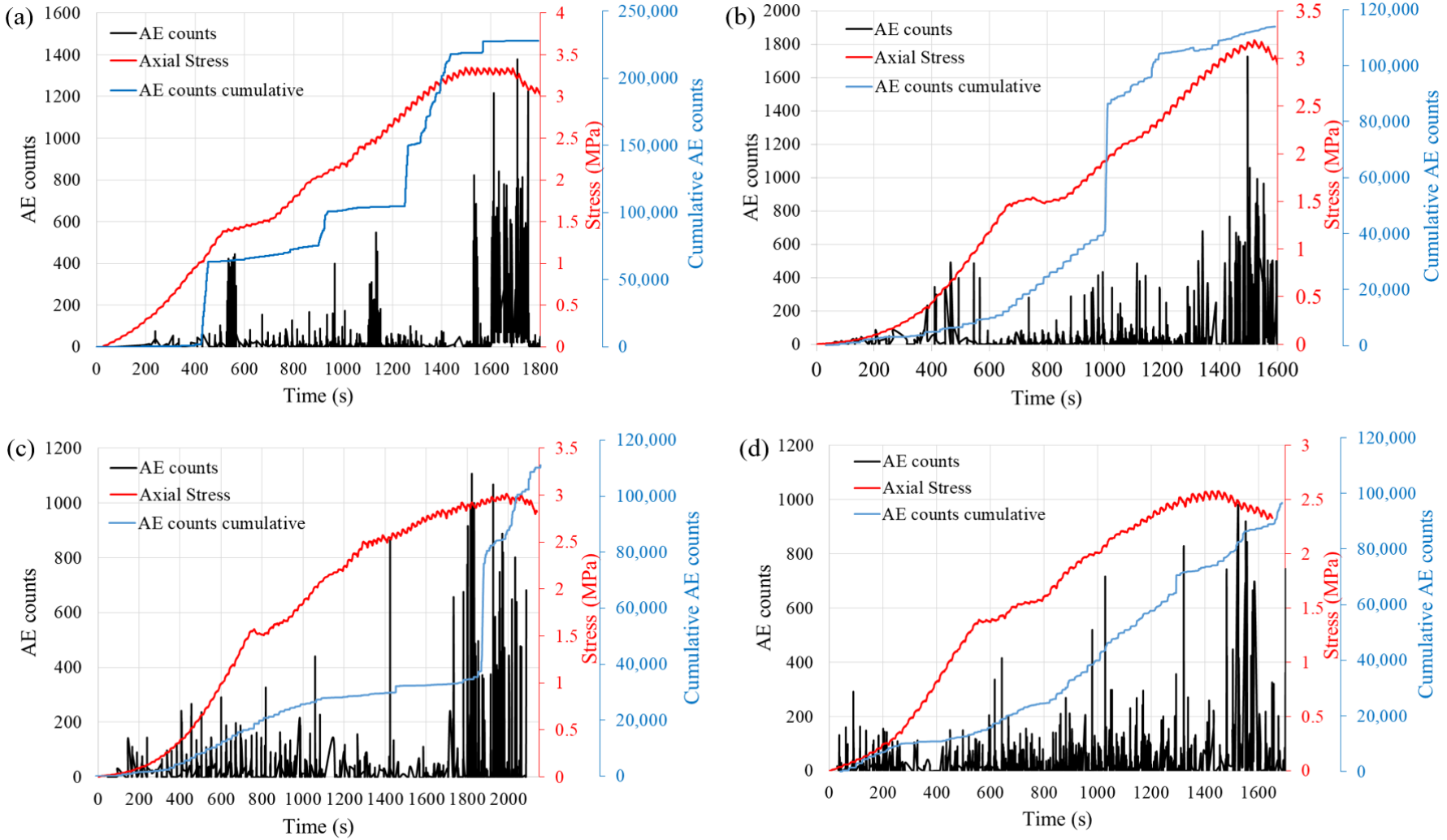

Figure 9. Compressive strength and acoustic emissions for different LN_2 treatments: (**a**) Baseline; (**b**) FT60 Specimen-1; (**c**) FT120 Specimen-1; and (**d**) FT180 Specimen-1.

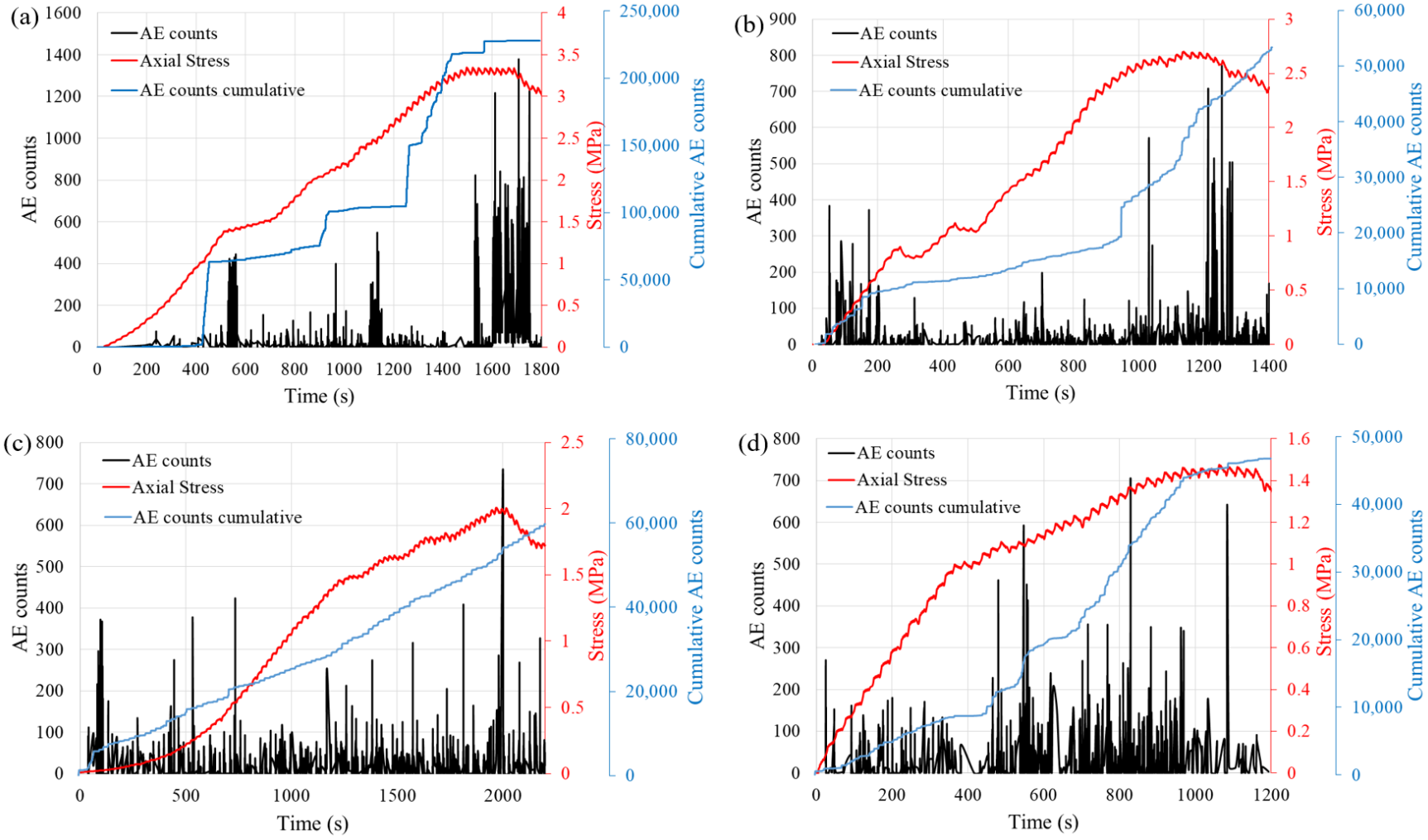

Figure 10. Compressive strength and acoustic emissions for different LN_2 treatments: (**a**) Baseline; (**b**) FTC2 Specimen-1; (**c**) FTC4 Specimen-1; and (**d**) FTC6 Specimen-1.

4.4. Limitations

While the results are believed to be representative of coal, they must still be considered in context.

- Due to the inability to obtain test samples from the field in the desired and expected shape for material testing, synthetic samples were prepared using common constituents.
- It is assumed that the measures of mechanical stress under compressive load are viable measures of altered sample strength, recognizing that the alteration was a result of thermal stress.
- Testing involving freezing and thawing cycles involved room temperature relaxation, rather than returning to the initial hot sample temperature, as in a downhole stimulation case. Thus, the impact of freezing–thawing cycles is underestimated.
- The exposure to LN_2 was by immersion only. In a downhole stimulation case, there would be injection and a combination of mechanical breakdown and thermal shock.

5. Conclusions

Various freezing techniques result in distinct variations in the mechanical properties of dry synthetic coal samples from the Karaganda Basin. The geological background was provided to facilitate the application of findings to comparable coal types. This involved the assessment of mechanical characteristics like acoustic emission, energy absorption, and peak compressive strength.

- During both freezing time and freezing–thawing cycles, coal specimens exhibit lower peaks in uniaxial compressive strength (UCS) as the time of LN_2 treatment increases. The mechanisms leading to mechanical weakening occur at the pore level and involve factors such as grain sorting, pressure, and temperature. However, it remains unclear whether a single mechanism prevails or if multiple mechanisms interact.
- Freezing–thawing specimens indicated lower UCS values compared to freezing time experiments. The damage factor decreases progressively in both freezing–thawing (FT) and freezing–thawing–cooling (FTC) experiments with an increase in the duration of LN_2 treatment.
- As the freezing time with liquid nitrogen (LN_2) extends, there is an observable rise in both the frequency and amplitude of acoustic emission (AE) signals. The coal samples fractured with LN_2 display increased fractures, leading to a sudden surge in AE counts and subsequently larger cumulative AE counts for the samples. Additionally, freezing–thawing (FT) processes show a higher and denser occurrence of signals compared to freezing–thawing–cooling (FTC) processes, indicating a positive correlation with uniaxial compressive strength (UCT) results.
- Analysis of energy absorption demonstrated a clear decrease in the strength of coal samples as freezing time and freezing–thawing cycles increased.

6. Future Research

Future research opportunities could examine the true temperature fluctuation in freezing–thawing experiments. Experiments with LN_2 exposure under confining pressure could result in fracture suppression or enhanced material breakdown from a combination of load and thermal expansion gradients. Research would also benefit from modeling the heat transfer processes and measures of temperature-dependent transport and geomechanical properties.

Author Contributions: Conceptualization, S.N.L.; methodology, S.N.L.; software, S.N.L. and A.S.; validation S.N.L. and A.S.; formal analysis, S.N.L.; investigation, S.N.L.; resources, S.N.L.; data curation, S.N.L.; writing—original draft preparation, S.N.L.; writing—review and editing, S.N.L., M.J., D.B. and R.H.; visualization, S.N.L.; supervision, E.B. and R.H.; project administration, R.H.; funding acquisition, E.B. All authors have read and agreed to the published version of the manuscript.

Funding: This research was funded by NAZARBAYEV UNIVERSITY, grant number 211123CRP1606, and the APC was funded by NAZARBAYEV UNIVERSITY.

Data Availability Statement: Data available upon request.

Acknowledgments: This present research was funded by Nazarbayev University through the Collaborative Research Program 2024–2026: 211123CRP1606.

Conflicts of Interest: The authors declare no conflict of ineterest.

References

1. Wang, H.; Asif Amjad, M.; Arshed, N.; Mohamed, A.; Ali, S.; Haider Jafri, M.A.; Khan, Y.A. Fossil energy demand and economic development in BRICS countries. *Front. Energy Res.* **2022**, *10*, 842793. [CrossRef]
2. Brics Energy Research Cooperation Platform. Energy Report. 2020. Available online: https://eng.brics-russia2020.ru/images/114/89/1148985.pdf (accessed on 15 March 2024).
3. Abbasi, K.R.; Shahbaz, M.; Zhang, J.; Irfan, M.; Alvarado, R. Analyze the environmental sustainability factors of China: The role of fossil fuel energy and renewable energy. *Renew. Energy* **2022**, *187*, 390–402. [CrossRef]
4. Holechek, J.L.; Geli, H.M.; Sawalhah, M.N.; Valdez, R. A global assessment: Can renewable energy replace fossil fuels by 2050? *Sustainability* **2022**, *14*, 4792. [CrossRef]
5. Ali, K.; Jianguo, D.; Kirikkaleli, D. How do energy resources and financial development cause environmental sustainability? *Energy Rep.* **2023**, *9*, 4036–4048. [CrossRef]
6. Merey, Ş.; Longinos, S. The gas hydrate potential of the Eastern Mediterranean basin. *Bull. miner. Res. Explor.* **2019**, *160*, 117–134. [CrossRef]
7. Chen, B.; Xiong, R.; Li, H.; Sun, Q.; Yang, J. Pathways for sustainable energy transition. *J. Clean. Prod.* **2019**, *228*, 1564–1571. [CrossRef]
8. Longinos, S.N.; Parlaktuna, M. Examination of methane hydrate formation by the use of dual impeller combinations. *React. Kinet. Mech. Catal.* **2021**, *133*, 729–740. [CrossRef]
9. Tao, Z.; Liu, C.; He, Q.; Chang, H.; Ma, J. Detection and treatment of organic matters in hydraulic fracturing wastewater from shale gas extraction: A critical review. *Sci. Total Environ.* **2022**, *824*, 153887. [CrossRef] [PubMed]
10. Kookana, R.S.; Williams, M.; Gregg, A.; Semmler, A.; Du, J.; Apte, S.C. Sorption, degradation and microbial toxicity of chemicals associated with hydraulic fracturing fluid and produced water in soils. *Environ. Pollut.* **2022**, *309*, 119754. [CrossRef]
11. Patterson, L.A.; Konschnik, K.E.; Wiseman, H.; Fargione, J.; Maloney, K.O.; Kiesecker, J.; Nicot, J.P.; Baruch-Mordo, S.; Entrekin, S.; Trainor, A.; et al. Unconventional oil and gas spills: Risks, mitigation priorities, and state reporting requirements. *Environ. Sci. Technol.* **2017**, *51*, 2563–2573. [CrossRef]
12. Yazdan, M.M.S.; Ahad, M.T.; Jahan, I.; Mazumder, M. Review on the evaluation of the impacts of wastewater disposal in hydraulic fracturing industry in the United States. *Technologies* **2020**, *8*, 67. [CrossRef]
13. Almaliki, A.J.D.; Bashir, M.J.; Llamas Borrajo, J.F. The Impact of Climate Change and Soil Classification on Benzene Concentration in Groundwater Due to Surface Spills of Hydraulic Fracturing Fluids. *Water* **2022**, *14*, 1202. [CrossRef]
14. Seidle, J. *Fundamentals of Coalbed Methane Reservoir Engineering*; PennWell Corporation: Tulsa, OK, USA, 2011.
15. Chu, Y.; Zhang, D.; Liu, H.; Wu, X.; Zhai, P.; Sheng, T. Experimental study on mechanical properties, acoustic emission characteristics and energy evolution of coal samples after freezing with liquid nitrogen. *Fuel* **2022**, *321*, 123955. [CrossRef]
16. Longinos, S.N.; Serik, A.; Zhang, D.; Wang, L.; Hazlett, R. Experimental Evaluation of Liquid Nitrogen Fracturing on the Coal Rocks in Karaganda Basin, Kazakhstan. *Arab. J. Sci. Eng.* **2023**, *48*, 16623–16638. [CrossRef]
17. Ali, M.; Shar, A.M.; Mahesar, A.A.; Al-Yaseri, A.; Yekeen, N.; Memon, K.R.; Keshavarz, A.; Hoteit, H. Experimental evaluation of liquid nitrogen fracturing on the development of tight gas carbonate rocks in the Lower Indus Basin, Pakistan. *Fuel* **2022**, *309*, 122192. [CrossRef]
18. Suárez, A.A. The expansion of unconventional production of natural gas (tight gas, gas shale and coal bed methane). In *Advances in Natural Gas Technology*; IntechOpen: London, UK, 2012; Volume 7.
19. Teng, T.; Wang, J.G.; Gao, F.; Ju, Y. Complex thermal coal-gas interactions in heat injection enhanced CBM recovery. *J. Nat. Gas. Sci. Eng.* **2016**, *34*, 1174–1190. [CrossRef]
20. Huang, Q.; Liu, S.; Wang, G.; Wu, B.; Yang, Y.; Liu, Y. Gas sorption and diffusion damages by guar-based fracturing fluid for CBM reservoirs. *Fuel* **2019**, *251*, 30–44. [CrossRef]
21. Roy, M.P.; Paswan, R.K.; Sarim, M.D.; Kumar, S.U.R.A.J.; Jha, R.; Singh, P.K. Rock fragmentation by blasting-A review. *J. mines Met. Fuels* **2016**, *64*, 424–431.
22. Zhang, Z.X. *Rock Fracture and Blasting: Theory and Applications*; Butterworth-Heinemann: Oxford, UK, 2016.
23. Al-Bakri, A.; Hefni, M. A review of some nonexplosive alternative methods to conventional rock blasting. *Open Geosci.* **2021**, *13*, 431–442. [CrossRef]
24. Siriwardane, H.J.; Bowes, B.D.; Bromhal, G.S.; Gondle, R.K.; Wells, A.W.; Strazisar, B.R. Modeling of CBM production, CO_2 injection, and tracer movement at a field CO_2 sequestration site. *Int. J. Coal Geol.* **2012**, *96*, 120–136. [CrossRef]

25. Kumar, H.; Elsworth, D.; Mathews, J.P.; Liu, J.; Pone, D. Effect of CO_2 injection on heterogeneously permeable coalbed reservoirs. *Fuel* **2014**, *135*, 509–521. [CrossRef]
26. Yang, X.; Wen, G.; Lu, T.; Wang, B.; Li, X.; Cao, J.; Lv, G.; Yuan, G. Optimization and field application of CO_2 gas fracturing technique for enhancing CBM extraction. *Nat. Resour. Res.* **2020**, *29*, 1875–1896. [CrossRef]
27. Lou, Y.; Song, H.; Yang, J.; Huang, X.; Dong, H. Productivity equation of fractured well in CBM reservoirs. *J. Nat. Gas Sci. Eng.* **2013**, *11*, 39–45. [CrossRef]
28. Feng, Q.; Liu, J.; Huang, Z.; Tian, M. Study on the optimization of fracturing parameters and interpretation of CBM fractured wells. *J. Nat. Gas Geosci.* **2018**, *3*, 109–117. [CrossRef]
29. Yang, S.; Cai, Y.; Wei, R.; Zhou, Y. A new fracture permeability model of CBM reservoir with high-dip angle in the southern Junggar Basin, NW China. *Energy Explor. Exploit.* **2019**, *37*, 125–143. [CrossRef]
30. Huang, Q.; Liu, S.; Wang, G.; Wu, B.; Zhang, Y. Coalbed methane reservoir stimulation using guar-based fracturing fluid: A review. *J. Nat. Gas Sci. Eng.* **2019**, *66*, 107–125. [CrossRef]
31. Sun, Z.; Huang, B.; Liu, Y.; Jiang, Y.; Zhang, Z.; Hou, M.; Li, Y. Gas-phase production equation for CBM reservoirs: Interaction between hydraulic fracturing and coal orthotropic feature. *J. Pet. Sci. Eng.* **2022**, *213*, 110428. [CrossRef]
32. Zhao, J.; Liu, P.; Li, J.; Chen, Z.; Li, Y.; Li, F. Fracture propagation induced by hydraulic fracturing using microseismic monitoring technology: Field test in CBM wells in Zhengzhuang region, Southern Qinshui Basin, China. *Front. Earth Sci.* **2023**, *11*, 1130280. [CrossRef]
33. Davies, R.; Foulger, G.; Bindley, A.; Styles, P. Induced seismicity and hydraulic fracturing for the recovery of hydrocarbons. *Mar. Pet. Geol.* **2013**, *45*, 171–185. [CrossRef]
34. Rutqvist, J.; Rinaldi, A.P.; Cappa, F.; Moridis, G.J. Modeling of fault reactivation and induced seismicity during hydraulic fracturing of shale-gas reservoirs. *J. Pet. Sci. Eng.* **2013**, *107*, 31–44. [CrossRef]
35. Schultz, R.; Skoumal, R.J.; Brudzinski, M.R.; Eaton, D.; Baptie, B.; Ellsworth, W. Hydraulic fracturing-induced seismicity. *Rev. Geophys.* **2020**, *58*, e2019RG000695. [CrossRef]
36. Atkinson, G.M.; Eaton, D.W.; Igonin, N. Developments in understanding seismicity triggered by hydraulic fracturing. *Nat. Rev. Earth Environ.* **2020**, *1*, 264–277. [CrossRef]
37. Liew, M.S.; Danyaro, K.U.; Zawawi, N.A.W.A. A comprehensive guide to different fracturing technologies: A review. *Energies* **2020**, *13*, 3326. [CrossRef]
38. Yu, H.; Xu, W.; Li, B.; Huang, H.; Micheal, M.; Wang, Q.; Huang, M.; Meng, S.; Liu, H.; Wu, H. Hydraulic fracturing and enhanced recovery in shale reservoirs: Theoretical analysis to engineering applications. *Energy Fuels* **2023**, *37*, 9956–9997. [CrossRef]
39. Farrokhrouz, M.; Akhondzadeh, H.; Yang, Y.; Awan, F.U.R.; Iglauer, S.; Lebedev, M.; Keshavarz, A. Coal cleat network stimulation through a combination of acidizing and liquid nitrogen fracturing. *Gas. Sci. Eng.* **2024**, 205308. [CrossRef]
40. Akhondzadeh, H.; Keshavarz, A.; AlYaseri, A.Z.; Ali, M.; Awan, F.U.R.; Wang, X.; Yang, Y.; Iglauer, S.; Lebedev, M. Pore-scale analysis of coal cleat network evolution through liquid nitrogen treatment: A Micro-Computed Tomography investigation. *Int. J. Coal Geol.* **2020**, *219*, 103370. [CrossRef]
41. Memon, K.R.; Mahesar, A.A.; Ali, M.; Tunio, A.H.; Mohanty, U.S.; Akhondzadeh, H.; Awan, F.U.R.; Iglauer, S.; Keshavarz, A. Influence of cryogenic liquid nitrogen on petrophysical characteristics of mancos shale: An experimental investigation. *Energy Fuels* **2020**, *34*, 2160–2168. [CrossRef]
42. Qin, L.; Zhai, C.; Liu, S.; Xu, J.; Yu, G.; Sun, Y. Changes in the petrophysical properties of coal subjected to liquid nitrogen freeze-thaw–a nuclear magnetic resonance investigation. *Fuel* **2017**, *194*, 102–114. [CrossRef]
43. Wang, S.; Su, S.; Wang, D.; Hou, P.; Xue, Y.; Liang, X.; Cai, C.; Gao, X.; Jin, Y.; Yang, S. Experimental study on fracture characteristics of coal due to liquid nitrogen fracturing. *Geomech. Energy Environ.* **2023**, *33*, 100438. [CrossRef]
44. Hou, P.; Su, S.; Gao, F.; Liang, X.; Wang, S.; Gao, Y.; Cai, C. Influence of liquid nitrogen cooling state on mechanical properties and fracture characteristics of coal. *Rock Mech. Rock Eng.* **2022**, *55*, 3817–3836. [CrossRef]
45. Yuan, Y.; Cai, F.; Yang, L. Pore structure characteristics and fractal structure evaluation of medium-and high-rank coal. *Energy Explor. Exploit.* **2022**, *40*, 328–342. [CrossRef]
46. Wu, X.; Li, H.; Lu, J.; Lu, Y.; Hong, Y.; Zheng, C.; Liu, M.; Lin, B.; Shi, S.; Wang, Z. Investigation of cross-scale characterization of porous structure and fluid index in bituminous coal via microwave-LN2 freeze-thaw cycles. *Fuel* **2024**, *357*, 129701. [CrossRef]
47. Zhai, C.; Qin, L.; Liu, S.; Xu, J.; Tang, Z.; Wu, S. Pore structure in coal: Pore evolution after cryogenic freezing with cyclic liquid nitrogen injection and its implication on coalbed methane extraction. *Energy Fuels* **2016**, *30*, 6009–6020. [CrossRef]
48. Longinos, S.N.; Dillinger, A.; Wang, L.; Hazlett, R. Uniaxial compressive strength (UCS) and SEM study of liquid nitrogen for waterless hydraulic fracturing in coalbed methane reservoirs of Karaganda Basin in Kazakhstan. *Gas Sci. Eng.* **2023**, *115*, 204998. [CrossRef]
49. Longinos, S.N.; Wang, L.; Hazlett, R. Advances in cryogenic fracturing of coal-bed methane reservoirs with LN2. *Energies* **2022**, *15*, 9464. [CrossRef]
50. Longinos, S.N.; Abbas, A.H.; Bolatov, A.; Skrzypacz, P.; Hazlett, R. Application of Image Processing in Evaluation of Hydraulic Fracturing with Liquid Nitrogen: A Case Study of Coal Samples from Karaganda Basin. *Appl. Sci.* **2023**, *13*, 7861. [CrossRef]
51. Li, B.; Zong, C.; Huang, L.; Ren, Y.; Lv, X. Study on the influence of liquid nitrogen cold soaking on the temperature variations and seepage characteristics of coal samples with different moisture contents. *Geofluids* **2021**, *2021*, 8924016. [CrossRef]

52. Li, B.; Huang, L.; Lv, X.; Ren, Y. Study on temperature variation and pore structure evolution within coal under the effect of liquid nitrogen mass transfer. *ACS Omega* **2021**, *6*, 19685–19694. [CrossRef] [PubMed]
53. Li, B.; Shi, Z.; Wang, Z.; Huang, L. Effect of liquid nitrogen freeze–thaw cycles on pore structure development and mechanical properties of coal. *ACS Omega* **2022**, *7*, 5206–5216. [CrossRef]
54. Cai, C.; Li, G.; Huang, Z.; Shen, Z.; Tian, S.; Wei, J. Experimental study of the effect of liquid nitrogen cooling on rock pore structure. *J. Nat. Gas Sci. Eng.* **2014**, *21*, 507–517. [CrossRef]
55. Cai, C.; Li, G.; Huang, Z.; Shen, Z.; Tian, S. Rock pore structure damage due to freeze during liquid nitrogen fracturing. *Arab. J. Sci. Eng.* **2014**, *39*, 9249–9257. [CrossRef]
56. Cai, C.; Li, G.; Huang, Z.; Tian, S.; Shen, Z.; Fu, X. Experiment of coal damage due to super-cooling with liquid nitrogen. *J. Nat. Gas Sci. Eng.* **2015**, *22*, 42–48. [CrossRef]
57. Qin, L.; Zhai, C.; Liu, S.; Xu, J. Factors controlling the mechanical properties degradation and permeability of coal subjected to liquid nitrogen freeze-thaw. *Sci. Rep.* **2017**, *7*, 3675. [CrossRef] [PubMed]
58. Qin, L.; Li, S.; Zhai, C.; Lin, H.; Zhao, P.; Shi, Y.; Bai, Y. Changes in the pore structure of lignite after repeated cycles of liquid nitrogen freezing as determined by nitrogen adsorption and mercury intrusion. *Fuel* **2020**, *267*, 117214. [CrossRef]
59. Sandström, T.; Fridh, K.; Emborg, M.; Hassanzadeh, M. The influence of temperature on water absorption in concrete during freezing. *Nord. Concr. Res.* **2012**, *45*, 45–58.
60. Han, S.; Cheng, Y.; Gao, Q.; Yan, C.; Han, Z. Experimental study of the effect of liquid nitrogen pretreatment on shale fracability. *J. Nat. Gas Sci. Eng.* **2018**, *60*, 11–23. [CrossRef]
61. Qu, H.; Li, C.; Qi, C.; Chen, X.; Xu, Y.; Jun, H.; Wu, X. Effect of liquid nitrogen freezing on the mechanical strength and fracture morphology in a deep shale gas reservoir. *Rock Mech. Rock Eng.* **2022**, *55*, 7715–7730. [CrossRef]
62. Mahesar, A.A.; Shar, A.M.; Ali, M.; Tunio, A.H.; Uqailli, M.A.; Mohanty, U.S.; Akhondza-deh, H.; Iglauer, S.; Keshavarz, A. Morphological and petro physical estimation of eocene tight carbonate formation cracking by cryogenic liquid nitrogen; a case study of Lower Indus basin, Pakistan. *J. Pet. Sci. Eng.* **2020**, *192*, 107318. [CrossRef]
63. Mahesar, A.A.; Ali, M.; Shar, A.M.; Memon, K.R.; Mohanty, U.S.; Akhondzadeh, H.; Tunio, A.H.; Iglauer, S.; Keshavarz, A. Effect of cryogenic liquid nitrogen on the morpho-logical and petrophysical characteristics of tight gas sandstone rocks from kirthar fold belt, Indus Basin, Pakistan. *Energy Fuels* **2020**, *34*, 14548–14559. [CrossRef]
64. Hong, C.; Yang, R.; Huang, Z.; Qin, X.; Wen, H.; Cong, R.; Liu, W.; Chen, J. Fracture initiation and morphology of tight sandstone by liquid nitrogen fracturing. *Rock Mech. Rock Eng.* **2022**, *55*, 1285–1301. [CrossRef]
65. Rong, G.; Sha, S.; Li, B.; Chen, Z.; Zhang, Z. Experimental investigation on physical and mechanical properties of granite subjected to cyclic heating and liquid nitrogen cooling. *Rock Mech. Rock Eng.* **2021**, *54*, 2383–2403. [CrossRef]
66. Longinos, S.N.; Hazlett, R. Cryogenic fracturing using liquid nitrogen on granite at elevated temperatures: A case study for enhanced geothermal systems in Kazakhstan. *Sci. Rep.* **2024**, *14*, 160. [CrossRef] [PubMed]
67. Longinos, S.N.; Tuleugaliyev, M.; Hazlett, R. Influence of subsurface temperature on cryogenic fracturing efficacy of granite rocks from Kazakhstan. *Geothermics* **2024**, *118*, 102919. [CrossRef]
68. Ivakhnenko, O.; Aimukhan, A.; Kenshimova, A.; Mullagaliyev, F.; Akbarov, E.; Mullagaliyeva, L.; Kabirova, S.; Almukhametov, A. Advances in coalbed methane reservoirs integrated characterization and hydraulic fracturing for improved gas recovery in Karaganda Coal Basin, Kazakhstan. *Energy Procedia* **2017**, *125*, 477–485. [CrossRef]
69. Sadykov, R.M.; Korobkin, V.V. Geological input data analysis for basin modeling of the south part of Karagandy coal deposit. *News Natl. Acad. Sci. Repub. Kazakhstan Ser. Geol. Tech. Sci.* **2019**, *1*, 133–142.
70. Château, C.; Fustic, M.; Duisekova, M. Geological carbon storage potential of Karagandy Basin, Kazakhstan. Abstract. In Proceedings of the 2nd EAGE Geoscience and Engineering for the Energy Transition Conference, Online, 23–25 November 2021; p. 5.
71. Kler, V.R. *Geology of the Karaganda Coal Basin*; Nedra. Geology of Coal and Oil Shale of the USSR: Moscow, Russia, 1973; Volume 9.
72. Kushev, G.L. *Karagandinskii Uglenosnyi Bassein 1963*, 2nd ed.; Alma-AtaMinistry of Industry and New Technologies of RoK. 2009: Innovative investment project "Methane" for 2010–2014; ministry of Industry and New Technologies of RoK: Astana, Kazakhstan, 2009. (In Russian)
73. Azizov, T.M.; Vlasov, Y.I. Coal and oil shale basins and deposits of Kazakhstan. A.B. Bekturov Institute of Chemical Sciences JSC: Almaty, Kazakhstan, 2013; pp. 6–106.
74. Sabitova, D.K. Exploration potential of coalbed methane in Karaganda field. *Mod. Appl. Sci.* **2015**, *9*, 145. [CrossRef]
75. Imanbaeva, S.B. Influences of Geological and mining Conditions of the D6 Coal Seam and Its Methane Concentration on the Efficiency of Rocks. Ph.D. Dissertation, Karagandy Technical University named after Abylqas Saginov, Karagandy, Kazakhstan, 2022. 163pyes (In Russian).
76. Tickner, J.; Roach, G. Characterisation of coal and minerals using compton profile analysis. *Nucl. Instrum. Methods Phys. Res.* **2004**, *213*, 507–510. [CrossRef]
77. Bo, L.; He, Q.; Jiang, Z.; Xu, R.; Hu, B. Relationship between coal ash composition and ash fu-sion temperatures. *Fuel* **2013**, *105*, 293–300.
78. Su, X.; Wang, Q.; Song, J.; Chen, P.; Yao, S.; Hong, J.; Zhou, F. Experimental study of water blocking damage on coal. *J. Petrol. Sci. Eng.* **2017**, *156*, 654–661. [CrossRef]

79. Wang, L. Clay stabilization in sandstone reservoirs and the perspectives for shale reservoirs. *Adv. Colloid. Interface Sci.* **2020**, *276*, 102087. [CrossRef]
80. Qin, L.; Zhai, C.; Liu, S.; Xu, J. Mechanical behavior and fracture spatial propagation of coal injected with liquid nitrogen under triaxial stress applied for coalbed methane recovery. *Eng. Geol.* **2018**, *233*, 1–10. [CrossRef]
81. Yang, R.; Hong, C.; Huang, Z.; Wen, H.; Li, X.; Huang, P.; Liu, W.; Chen, J. Liq-uid nitrogen fracturing in boreholes under true triaxial stresses: Laboratory investigation on fractures initiation and morphology. *SPE J.* **2021**, *26*, 135–154. [CrossRef]
82. Zhao, X.; Wang, L.; Yao, B.; Cha, M.; Wu, Y.S. Cryogenic fracturing of syn-thetic coal specimens under true-triaxial loadings-An experimental study. *Fuel* **2022**, *324*, 124530. [CrossRef]
83. Sass, O. Rock moisture fluctuations during freeze-thaw cycles: Preliminary results from electrical resistivity measurements. *Polar Geogr.* **2004**, *28*, 13–31. [CrossRef]
84. Tan, X.; Chen, W.; Liu, H.; Wang, L.; Ma, W.; Chan, A.H.C. A unified model for frost heave pressure in the rock with a penny-shaped fracture during freezing. *Cold Reg. Sci. Technol.* **2018**, *153*, 1–9. [CrossRef]
85. Qin, L.; Zhai, C.; Xu, J.; Liu, S.; Zhong, C.; Yu, G. Evolution of the pore structure in coal subjected to freeze− thaw using liquid nitrogen to enhance coalbed methane extraction. *J. Pet. Sci. Eng.* **2019**, *175*, 129–139. [CrossRef]
86. Qin, L.; Ma, C.; Li, S.; Lin, H.; Ding, Y.; Liu, P.; Wang, P.; Gao, Z. Liquid nitrogen's effect on the mechanical properties of dried and water-saturated frozen coal. *Energy Fuels* **2022**, *36*, 1894–1903. [CrossRef]
87. Wen, H.; Yang, R.; Huang, Z.; Hu, X.; Hong, C.; Song, G. Flow and heat transfer of nitrogen during liquid nitrogen fracturing in coalbed methane reservoirs. *J. Pet. Sci. Eng.* **2022**, *209*, 109900. [CrossRef]
88. Akhondzadeh, H.; Keshavarz, A.; Awan, F.U.R.; Ali, M.; Al-Yaseri, A.; Liu, C.; Yang, Y.; Iglauer, S.; Gurevich, B.; Lebedev, M. Liquid nitrogen fracturing efficiency as a function of coal rank: A multi-scale tomographic study. *J. Nat. Gas Sci. Eng.* **2021**, *95*, 104177. [CrossRef]
89. Akhondzadeh, H.; Keshavarz, A.; Awan, F.U.R.; Zamani, A.; Iglauer, S.; Lebedev, M. Coal cleat network evolution through liquid nitrogen freeze-thaw cycling. *Fuel* **2022**, *314*, 123069. [CrossRef]
90. Chu, Y.; Zhang, D. Study on the pore evolution law of anthracite coal under liquid nitrogen freeze-thaw cycles based on infrared thermal imaging and nuclear magnetic resonance. *Energy Sci. Eng.* **2019**, *7*, 3344–3354. [CrossRef]
91. Sun, L.; Wu, C.; Teng, T.; Cao, Z.; Liu, F.; Cai, Y.; Xue, Y.; Zhu, Y. Investigation of the impact of heating and liquid nitrogen (LN2) cooling on the mechanical and acoustic emission (AE) properties of coal. *Energy Explor. Exploit.* **2024**. [CrossRef]

Disclaimer/Publisher's Note: The statements, opinions and data contained in all publications are solely those of the individual author(s) and contributor(s) and not of MDPI and/or the editor(s). MDPI and/or the editor(s) disclaim responsibility for any injury to people or property resulting from any ideas, methods, instructions or products referred to in the content.